THE JOURNAL OF PHYSICAL CHEMISTRY C

ARTICLE

pubs.acs.org/JPCC

Shape Evolution and Gram-Scale Synthesis of Gold@Silver Core−Shell Nanopolyhedrons

Garam Park,[†] Daeha Seo,[†] Jongwook Jung,[†] Seol Ryu,[*,‡] and Hyunjoon Song[*,†]

[†]Department of Chemistry, Korea Advanced Institute of Science and Technology, Daejeon, 305-701, Korea

[‡]Department of Chemistry, Chosun University, Gwangju, 501-759, Korea

Supporting Information

ABSTRACT: Au@Ag heterometal core−shell nanoparticles with distinct polyhedral shapes were successfully synthesized by a seed-mediated polyol process on a gram scale. The addition of the silver precursor solution led to continuous shape evolution from gold seeds to silver spheres, cuboctahedrons, and cubes, respectively. Silver nanocubes were also grown by selective edge growth on gold cuboctahedral seeds. The overgrowth of silver shells could precisely tune the optical properties of the core−shell polyhedrons. Interestingly, a large red-shift of the extinction peak from that of the gold seeds was observed in the Au cuboctahedron@Ag cubes, reflecting a combination of composition and shape effects.

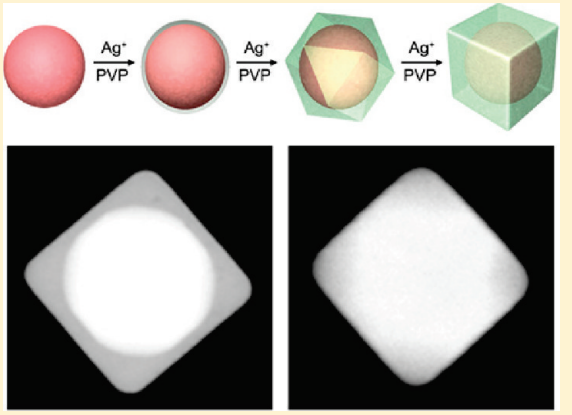

INTRODUCTION

Bimetallic nanoparticles are currently of much interest because of their physical properties distinct from a simple combination of each metal component.[1,2] Among the bimetallic nanostructures, core−shell type nanoparticles have been widely studied in order to utilize the multiple functionality of independent domains.[3] Synergistic effects between core and shell materials enabled the chemical and physical properties to be exhibited better than those of the single component.[4−8] Most of the core−shell nanoparticles have been based on concentric spheres, but since Yang et al. demonstrated epitaxial formation of binary metal polyhedrons, metal@metal core−shell polyhedral structures have widely been studied thus far.[9,10]

Among different combinations of metals, gold−silver and gold−palladium binary systems are suitable for the synthesis of well-defined polyhedral structures.[11] In particular, gold and silver are representative noble metals and have analogous physical and chemical properties such as high electric conductivity and ductility. They have similar lattice constants with a small lattice mismatch (0.2%) that leads to heteroepitaxial growth on the surface. Because of distinct dielectric constants, gold and silver strongly scatter light in different wavelengths, and thus mixing of the gold and silver components can precisely tune optical signatures in the visible range.[12−14] Consequently, gold−silver bimetallic structures are a central topic, owing to their structural and optical tunability. Tian et al. reported the growth of silver cubes from gold octahedrons,[11] and Xia et al. recently synthesized Au@Ag core−shell nanocubes with controllable shell thicknesses.[15] Silver octahedrons were successfully grown from gold nanorods,[16,17] and plate-like silver structures were also obtained from gold seeds.[18−20] Other core−shell type structures were reported as mixtures.[21,22] We have also reported a selective growth of silver nanorods and wires from gold dodecahedral seeds.[23,24] However, structural variation of nanostructures by simple synthetic methods and large scale synthesis are still required for potential applications.

In the present work, we report on synthesis of Au@Ag core−shell nanoparticles with distinct polyhedral shapes. Silver shells were epitaxially grown from gold spherical seeds, and continuous growth of the silver subsequently yielded cubes, cuboctahedrons, and octahedrons under polyol synthesis conditions, respectively. The core−shell nanoparticles could be synthesized on a gram scale by proportional increase of the amounts of precursors and solvents. Silver nanocubes were also grown by selective edge growth on gold cuboctahedral seeds. Such overgrowth of silver shells could precisely tune the optical properties of the core−shell polyhedrons. Interestingly, a large red-shift of the extinction peak from that of the gold seeds was observed in the Au cuboctahedron@Ag cubes, reflecting a combination of composition and shape effects.

EXPERIMENTAL SECTION

Reagents. Tetrachloroaurate trihydrate ($HAuCl_4 \cdot 3H_2O$, 99.9+%, Aldrich), silver nitrate ($AgNO_3$, 99+%, Aldrich), poly(vinyl

Received: January 12, 2011
Revised: March 17, 2011
Published: April 27, 2011

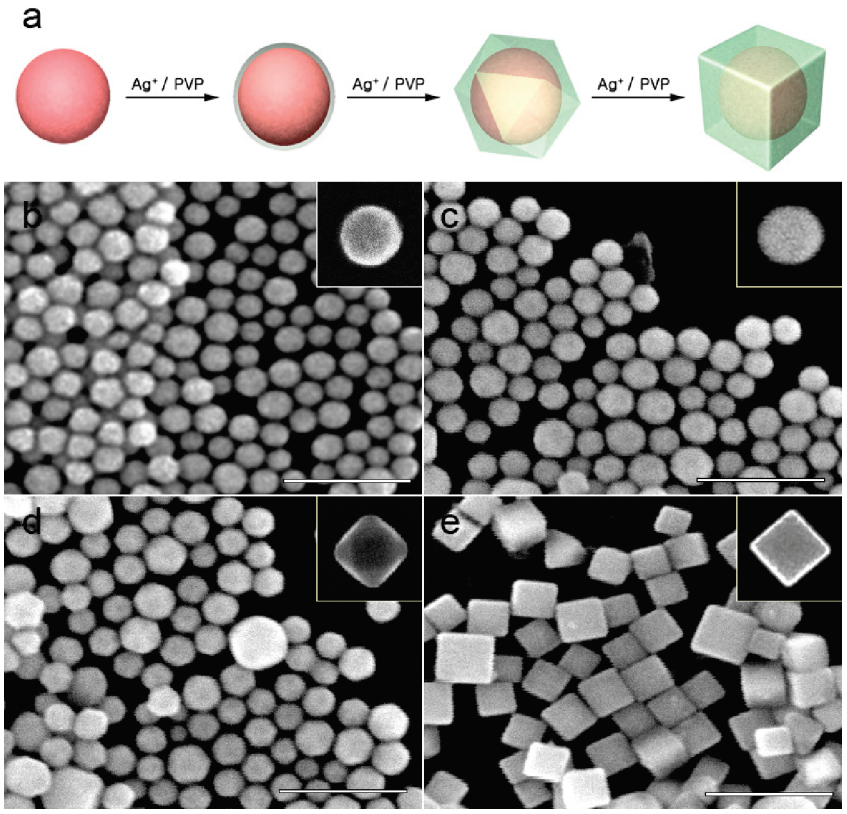

Figure 1. (a) Synthesis of Au@Ag core−shell nanopolyhedrons. SEM images of (b) gold spherical seeds, (c) Au@Ag spheres, (d) Au@Ag cuboctahedrons, and (e) Au@Ag cubes. The bars represent 200 nm.

pyrrolidone) (PVP, M_w = 55 000, Aldrich), 1,5-pentanediol (PD, 96%, Aldrich), diethylene glycol (DEG, 99%, Aldrich), and nitric acid (HNO_3, 60−61%, Junsei) were used as received.

Synthesis of Gold Spherical Seeds. A $AgNO_3$ solution in PD (0.15 mL, 0.020 M) was added to boiling PD (31 mL). Then PVP (6.0 mL, 0.15 M) and $HAuCl_4$ (3.0 mL, 0.05 M) solutions in PD were periodically added every 30 s over 7.5 min. The resulting mixture was refluxed for 1 h. The product was purified by a repetitive dispersion/precipitation cycle with ethanol and was finally dispersed in ethanol (30 mL) for further reactions. The average diameter of the gold spheres was estimated to be 43 ± 7 nm.

Synthesis of Au Sphere@Ag Polyhedrons. The gold seed dispersion in DEG (1.0 mL, 0.025 M with respect to the gold precursor concentration) was prepared by exchanging the solvent with centrifugation. The seed dispersion (1.0 mL), nitric acid (11 μL, 0.24 M), PVP (1.0 mL, 0.15 M), and $AgNO_3$ (1.0 mL, 0.051 M) solutions in DEG were added to DEG (4.0 mL) at 160 °C. The mixture was stirred at 160 °C for 1 min (Ag spheres), 5 min (Ag cuboctahedrons), and 30 min (Ag cubes), respectively. After cooling the reaction mixture, the product was purified by a repetitive dispersion/precipitation cycle with ethanol.

Synthesis of Gold Cuboctahedral Seeds. The gold seed dispersion in PD (1.0 mL, 0.013 M with respect to the gold precursor concentration) was added to boiling PD (4.0 mL). Then PVP (3.0 mL, 0.038 M) and $HAuCl_4$ (3.0 mL, 0.013 M) solutions in PD were periodically added every 30 s over 7.5 min. The particles were precipitated by centrifugation and were redispersed in ethanol (30 mL). The average diameter of the gold cuboctahedrons was estimated to be 65 ± 8 nm.

Synthesis of Au Cuboctahedron@Ag Cubes. The gold seed dispersion in DEG (1.0 mL, 8.5 mM) was prepared by exchanging the solvent with centrifugation. The seed dispersion (1.0 mL), PVP (1.0 mL, 0.01 M), and $AgNO_3$ (1.0 mL, 0.0017 M) solutions in DEG were added to DEG (4.0 mL) at 200 °C. The resulting mixture was stirred at 200 °C for 1 h. After cooling the reaction mixture, the product was purified by a repetitive dispersion/precipitation cycle with ethanol.

Gram-Scale Synthesis of Au@Ag Core−Shell Polyhedrons. For the gram-scale synthesis of Au@Ag cubes, the gold seed dispersion in DEG (65 mL, 0.051 M with respect to the gold precursor concentration), nitric acid (0.25 mL, 2.3 M), and PVP (11 mL, 0.90 M) and $AgNO_3$ (33 mL, 0.10 M, 0.36 g) solutions in DEG were added to DEG (250 mL) at 160 °C, and the mixture was stirred at the same temperature for 1 h. After cooling the reaction mixture, the product was purified by a repetitive dispersion/precipitation cycle with ethanol. For the synthesis of other Au@Ag polyhedrons, the amounts of the reagents used in the reactions were the gold seed dispersions in DEG (100 mL, 0.050 M; 90 mL, 0.050 M; 80 mL, 0.050 M), nitric acid (0.028 mL, 2.3 M; 0.084 mL, 2.3 M; 0.18 mL, 2.3 M), PVP (1.3 mL, 0.90 M; 3.8 mL, 0.90 M; 8.0 mL, 0.90 M), and $AgNO_3$ (3.8 mL, 0.10 M, 0.041 g; 11.3 mL, 0.10 M, 0.12 g; 24 mL, 0.10 M, 0.26 g) in DEG, and DEG (380 mL; 340 mL; 300 mL), for Au@Ag spheres, Au@Ag cuboctahedrons, and Au cuboctahedron@Ag cubes, respectively.

Characterization. SEM images were obtained using a Philips XL30S FEG operated at 10 kV. Transmission electron microscopy (TEM) and high resolution TEM (HRTEM) images, selected area electron diffraction (SAED) patterns,

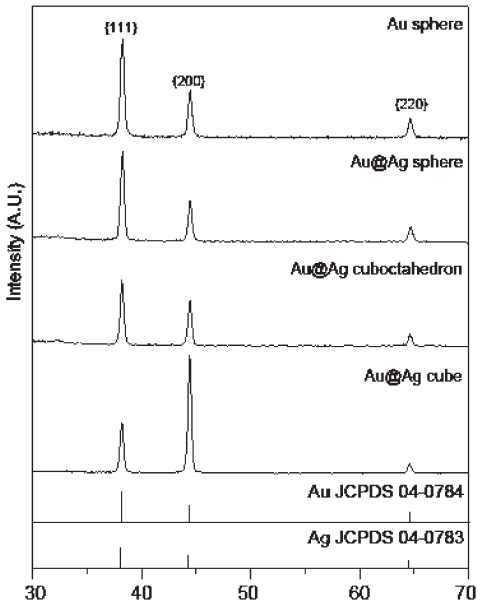

Figure 2. X-ray diffraction data of gold spheres and Au@Ag core−shell nanopolyhedrons.

energy dispersive X-ray spectroscopy (EDX) spectra, and line profiles were acquired on a JEOL FB-2100F (HR) operated at 200 kV at National Nanofabrication Center at KAIST. X-ray diffraction (XRD) patterns were recorded on a Rigaku D/max-IIIC (3 kW) diffractometer using Cu Kα radiation. The samples were prepared by a few drops of the colloidal solutions in ethanol either on copper grids coated with lacey carbon film (Ted Pella, Inc.) for TEM, or on small pieces (5 mm ×5 mm) of silicon wafer (P-100) for SEM and XRD and were allowed to dry in air. The UV−vis absorption data were recorded on a Jasco V670 UV−vis-NIR spectrophotometer using colloidal ethanol suspensions.

Theoretical Simulation. The calculated spectra for sphere-shaped nanoparticles (the first two structures in Figure S4, Supporting Information) were obtained using the Mie theory,[25] and theoretical works for the other Au@Ag core−shell nanopolyhedrons were carried out using discrete dipole approximation (DDA).[26] For the DDA calculations, we modeled four three-dimensional nanopolyhedral geometries using cubic point dipoles. The Au@Ag cuboctahedron having an average diameter of 46 nm of the sphere circumscribing the structure was constructed with 63327 point dipoles after the tip-point apexes and edges of the cuboctahedron were snipped by one point dipole at the planes perpendicular to their pointing directions. The Au@Ag cube having an edge length of 55 nm was con structed with 155 616 point dipoles after the tip-point apexes and edges were snipped by 4-point dipoles. In the center of these two nanopolyhedral structures, a gold nanosphere having a diameter of 43 nm was defined as the gold seed portion with 38 641 point dipoles. The gold cuboctahedron having an average diameter of 65 nm of the sphere circumscribing the structure was constructed with 24 117 point dipoles after the apexes and edges of the cuboctahedron were snipped by a one point dipole. The Au cuboctahedron@Ag cube having an edge length of 72 nm was constructed with 28 763 point dipoles after the apexes and edges were snipped by a one point dipole. The spectra were averaged over 64 orientations of the nanopolyhedra with respect to the direction of incident light,

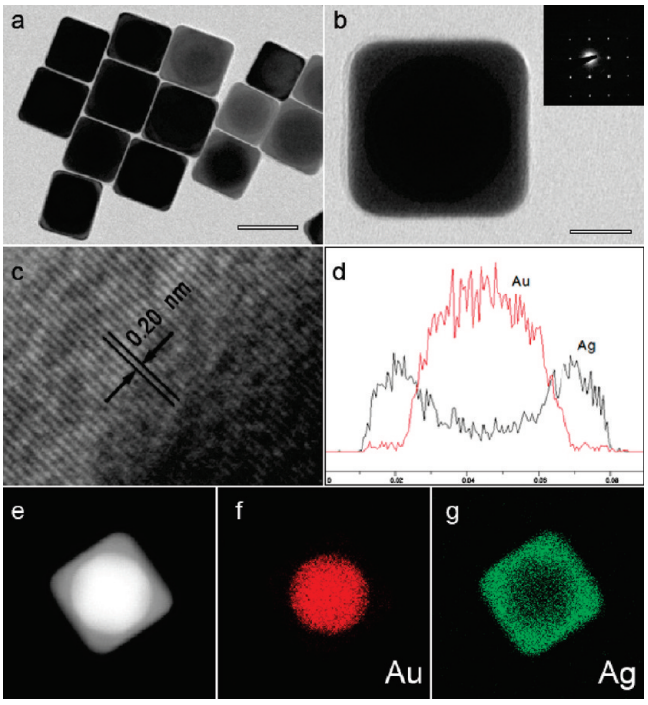

Figure 3. (a) TEM image of Au@Ag cubes, (b) TEM image and SAED pattern of a single Au@Ag cube, (c) HRTEM image of a nanocube at the boundary of gold and silver domains, (d) line profile analysis of gold and silver along a diagonal of one face, (e) HAADF-STEM image, and elemental mapping of (f) gold at 2.120 keV and (g) silver at 2.984 keV of a single nanocube. The bars represent (a) 50 nm and (b) 20 nm.

and the wavelength of light was increased from 400 to 800 nm by 1 nm. The refractive index values for gold and silver were obtained from the literature.[27]

RESULTS AND DISCUSSION

Au@Ag core−shell polyhedrons were synthesized via a two-step reduction of gold and silver precursors (Figure 1a). Gold spherical seeds with an average diameter of 43 ± 7 nm were synthesized by the reduction of $HAuCl_4$ in boiling 1,5-pentanediol (PD) in the presence of poly(vinylpyrrolidone) (PVP) (Figure 1b).[28] The gold seed dispersion and $AgNO_3$, HNO_3, and PVP solutions in diethylene glycol (DEG) were simultaneously added to DEG at 160 °C, and the mixture was stirred at the same temperature. The reactions were quenched at 1 min and every 5 min after the addition of the reactants, and the products were isolated by centrifugation. The scanning electron microscopy (SEM) images in Figure 1c−e showed uniform shape evolution of the silver shells along the reaction progress. For the sample quenched at 1 min, the product was still spherical without diameter change from the original gold seeds (Figure 1c, average diameter of 43 ± 5 nm). However, the energy dispersive X-ray spectroscopy (EDX) analysis exhibited a significant increase of the silver content (7 mol %, Figure S1, Supporting Information). The X-ray photoelectron spectrum (XPS) estimated 30 mol % of silver with respect to the total metal content, indicating that most of the silver components were located on the particle surface. If all the silver atoms were evenly deposited to form a silver shell, the shell thickness was estimated to be ~0.4 nm, which was hardly detectable in the SEM image.

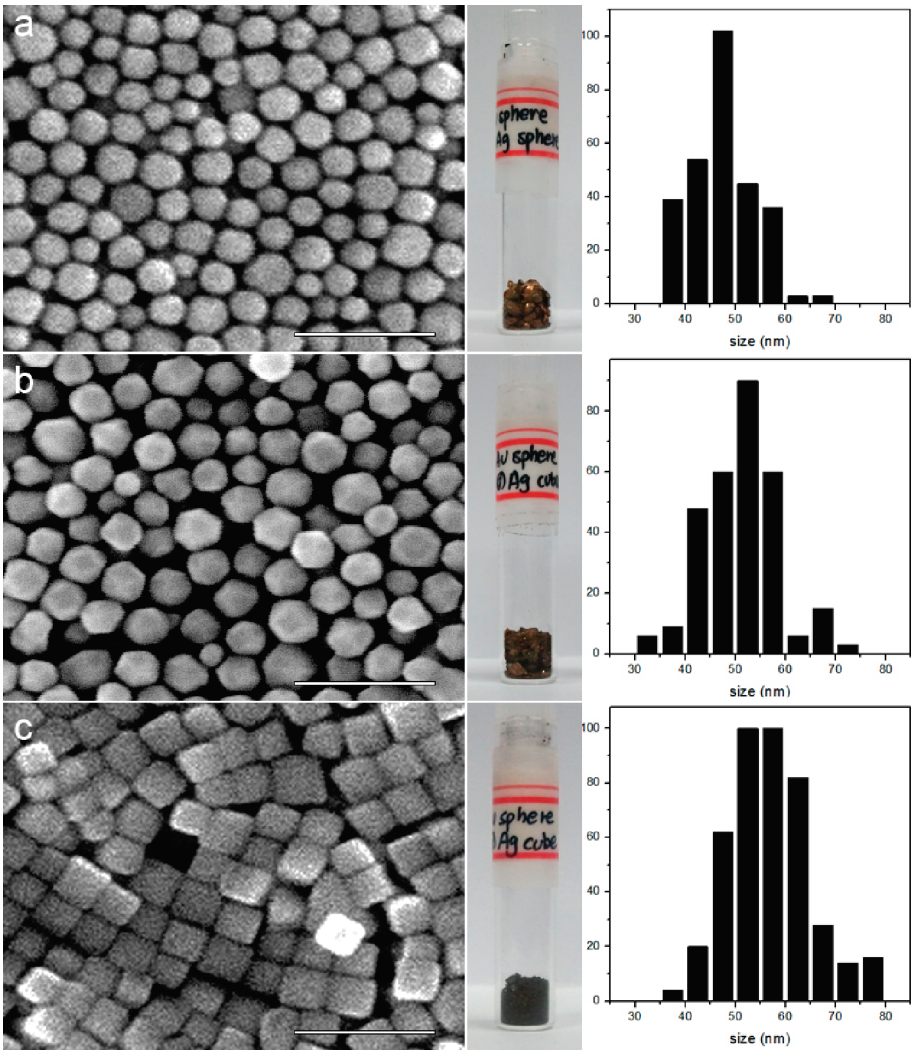

Figure 4. SEM images, photographs of powder forms, and size distribution histograms of Au@Ag core−shell (a) spheres, (b) cuboctahedrons, and (c) cubes synthesized in gram scales. The bars represent 200 nm.

The sample with the reaction period of 5 min was composed of faceted nanoparticles with mostly hexagonal projections in the SEM image (Figure 1d). The high resolution SEM image of a single particle (inset) showed an ideal cuboctahedral structure. The average diameter was estimated to be 46 ± 5 nm by assuming a sphere circumscribing each polyhedral structure. The EDX analysis estimated 19 mol % of silver with respect to the total metal content. The samples quenched at every 5 min from 10 to 25 min showed continuous edge growth of silver shells from cuboctahedrons to cubes (Figure S2, Supporting Information). A longer reaction time of up to 30 min yielded fully developed nanocubes with sharp edges (Figure 1e). The average edge length was estimated to be 54 ± 3 nm, which could be converted to 47 nm of the diameter of the circumscribed spheres. This value was nearly identical to that of the cuboctahedrons, indicating exclusive edge (or vertex) growth of the silver layers. The silver precursor was completely consumed within 30 min, and the nanocubes maintained their structure at the reaction time longer than 30 min. The X-ray diffraction (XRD) data of the gold@silver polyhedrons represented facets that dominated the surface as well as spontaneous orientation of the polyhedrons (Figure 2). The gold spherical seeds and the gold@silver spheres had typical intensity ratios between {111}, {200}, and {220} peaks. However, the ratio of {200}/{111} largely increased in the Au@Ag cuboctahedrons, and the {200} peak became the most intense peak in the Au@Ag cubes, reflecting the increment of {100} facets on the polyhedral surface.[29]

For the Au@Ag nanocubes, the transmission electron microscopy (TEM) images showed that each nanocube had a dark spherical core at the center (Figure 3a). Figure 3b showed a 52 nm-edged single cube including a spherical core with a diameter of 45 nm. A concentric arrangement of the cubic shell and the spherical core indicated symmetric growth of silver on the gold surface. The selected area electron diffraction (SAED) pattern along the zone axis normal to the {100} face (Figure 3b inset) and continuous lattice fringes in the high resolution TEM image at the silver−gold boundary (Figure 3c) strongly supported silver growth through an epitaxial fashion during the reaction. The average lattice spacing between adjacent fringes was 0.20 nm that corresponded to distance of silver and gold {200} crystallographic planes. The EDX analysis at different positions (Figure S3, Supporting Information) and the line profile along the diagonal of one face (Figure 3d) indicated that the silver shell and gold core regions were clearly distinguished without forming

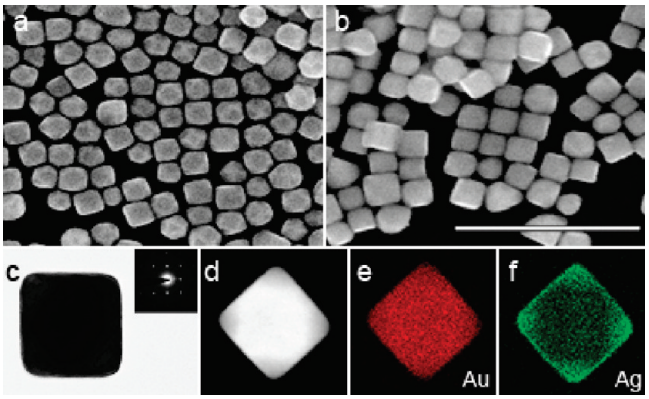

Figure 5. SEM images of (a) gold cuboctahedron seeds and (b) Au cuboctahedron@Ag cubes. (c) TEM image, (inset) SAED pattern, and (d) HAADF-STEM image of a single Au cuboctahedron@Ag cube, and elemental mapping of (e) gold and (f) silver. The bar represents 500 nm.

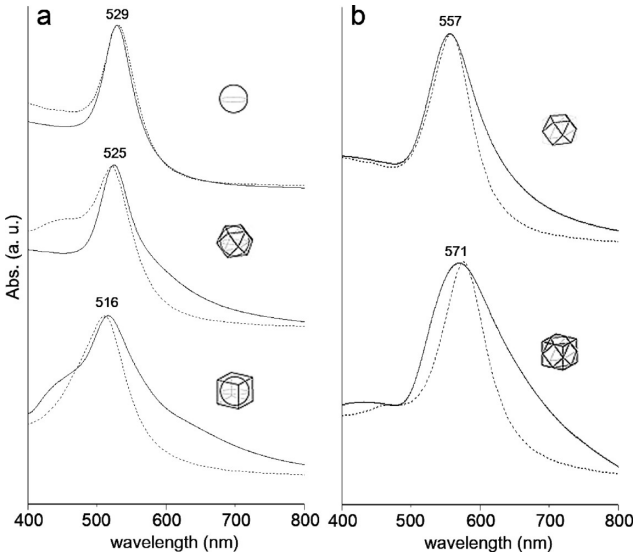

Figure 6. UV−vis extinction spectra (solid lines) and DDA calculation results (dotted lines) of (a) gold spherical seeds, Au@Ag cuboctahedrons, and Au@Ag cubes, and (b) gold cuboctahedral seeds and Au cuboctahedron@Ag cubes.

Ag−Au alloys. The high angle annular dark field-scanning transmission electron microscopy (HAADF-STEM) also showed a bisegmental feature of the Au@Ag nanocube (Figure 3e). Elemental mapping of silver and gold exhibited separated distribution of the components with the shapes of gold sphere and silver shell, respectively.

For the Au@Ag cuboctahedrons, the TEM image of a single particle represented selective edge growth of the silver component to form either cubic or hexagonal projections of the particles (Figure S4, Supporting Information). A typical cubic SAED pattern along the zone axis normal to {100} was observed in the particle with a cubic projection.

Difficulty in large-scale synthesis of well-designed nanostructures has always been a major drawback for applications.[30,31] The synthesis scale of the Au@Ag core−shell polyhedrons was readily extended to a gram-scale, because silver overgrowth on the gold seeds was carried out via a one-step process. Proportional increase of the gold seed and reagent concentrations yielded a gram of the Au@Ag core−shell polyhedrons. Figure 4 showed good quality of the large-scale products in size and shape distributions. The resulting particles were isolated as a powder form, which could be redispersed well in ethanol by the help of short sonication treatment. The average sizes and size distributions of Au@Ag spheres, cuboctahedrons, and cubes on gram scales were estimated to be 47 ± 7, 51 ± 8, and 57 ± 8 nm, respectively, and were depicted as histograms in Figure 4, where the average size of cuboctahedrons was obtained from the average diameter of circumscribed spheres covering edges and faces of the cuboctahedrons. The average sizes were consistent, and the size distributions were not much broadened compared to the values of polyhedrons produced in small scales. This readily scalable synthesis is one of the excellent advantages in the polyol-type process, in which the synthetic method is one-step and easy, and the reaction kinetics are precisely controlled by adjusting reaction temperatures.

The selective overgrowth of silver was also employed for gold polyhedral cores. For instance, silver cubes were grown from gold cuboctahedrons. Figure 5a and 5b showed gold cuboctahedrons and Au cuboctahedron@Ag cubes, respectively. The average diameter of the circumscribed spheres of the gold cuboctahedrons was estimated to be 65 ± 8 nm, and the average edge length of the resulting Au@Ag cubes were 72 ± 5 nm. The TEM image of a single cube had a dark diamond pattern inside a square projection, indicating a regular orientation of the gold face. A clear cubic pattern of the SAED spots indicated epitaxial relationship of gold and silver domains (Figure 5 inset). The HAADF-STEM image and elemental mapping of gold and silver showed that both domains were clearly distinguished without alloy formation, and the silver component mostly occupied areas near to the vertices. By considering the original cuboctahedral structure, silver growth selectively occurred on the gold {111} facets to form edges and vertices of the final silver cubes. The Au cuboctahedron@Ag cubes were also successfully synthesized on a gram scale without significant change of their average size and size distributions (Figure S5, Supporting Information).

This selective overgrowth was due to preferential adsorption of PVP on the silver {100} facets.[20] The silver precursor was reduced by DEG at high temperature to form silver species (mostly Ag_4^{2+}) and silver(0) nanoparticles.[28,32] These species were deposited on the gold seed surface through a heteroepitaxial way, aligning atomic arrangement between gold and silver (Figure 3c),[24] in order to lower interfacial energy.[9,10] Then PVP was selectively adsorbed on the Ag{100} facets and suppressed the {100} growth rate and/or enhanced the growth rates of other facets such as {111} and {110}. As a result, the outer structure became cubes with all exposed facets of {100}, when the reaction was complete.

The silver shell formation on the gold cores could precisely tune light extinction in the visible region. In previous results on Au@Ag core−shell nanoparticles, the SPR band continuously shifted from that of pure gold nanoparticles (~520 nm) to that of silver nanoparticles (~400 nm) by increasing the silver content.[12−14,33,34] The present Au sphere@Ag polyhedrons exhibited 4 and 13 nm blue-shifts of the maximum peaks for silver cuboctahedrons and cubes, respectively (Figure 6a), indicating that the increment of the silver component altered dielectric constants closer to that of bulk silver.[27] These overall blue-shifts observed for the Au sphere@Ag polyhedrons were contrary to the morphology effect, in which the size enlargement and shape deviation from spheres led to red-shifts of the extinctions.[35,36]

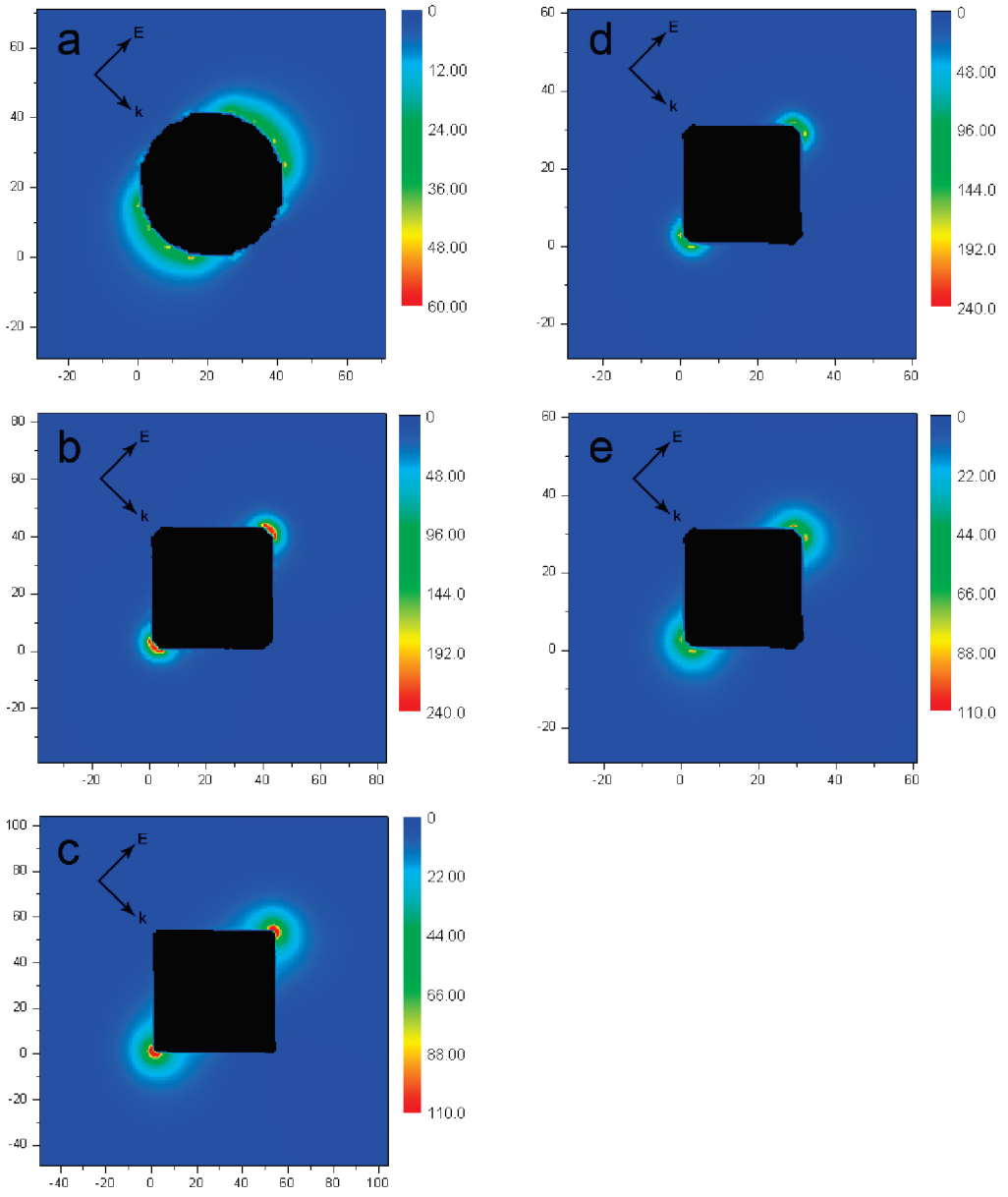

Figure 7. Electric field distribution $|\mathbf{E}|^2/|\mathbf{E}_0|^2$ of (a) a gold sphere, (b) a Au@Ag cuboctahedron, (c) a Au@Ag cube, (d) a gold cuboctahedron, and (e) a Au cuboctahedron@Ag cube. The *x* and *y* axes in each map are the number of dipoles. **k** is the wave vector, and **E** is the electric-field polarization of light. Electric field distributions were calculated at the major peak wavelengths of (a) 530, (b) 523, (c) 511, (d) 558, and (e) 577 nm, respectively.

However, it is not unnatural that the particles covered with a silver surface tend to optically behave as silver nanoparticles, if we consider the fact that optical properties of metal nanoparticles are determined by surface plasmon resonances. In these cases, the shell composition effect on the optical properties outweighs the morphology effect.

In the case of gold cuboctahedral cores, however, silver cubic shells provided a large red-shift (14 nm, Figure 6b), although the silver component was added to the gold surface. This opposite trend can be elucidated with the combination of composition and morphology effects as well. Our DDA simulation results indicated that ~50 nm red-shift was expected when the gold cuboctahedron seed grew to the gold cube, while ~35 nm blue-shift was obtained by switching the grown portion from gold to silver. Therefore, the 14 nm red-shift in the Au cuboctahedron@Ag cubes can be explained by the fact that the morphology effect outweighs the shell composition effect.

The theoretical extinction curves provided by DDA calculation matched well with the experimental data in all structures (dotted curves in Figure 6).[26] Both the blue-shifts of the Au sphere@Ag polyhedrons and the red-shifts of the Au cuboctahedron@Ag cubes by growing the silver shells were well supported. The spectral features of absorption and scattering following blue- or red-shifts of the corresponding core−shell structures could also be observed (Figure S6, Supporting Information). It is noteworthy that far-field properties such as extinction, absorption, and scattering can be modulated with such core−shell or surface heterodomain structures.

We calculated the normalized squared electric field distribution, $|\mathbf{E}|^2/|\mathbf{E}_0|^2$, near the polyhedral nanoparticles, at the maximum

dx.doi.org/10.1021/jp200338p |*J. Phys. Chem. C* 2011, 115, 9417–9423

extinction wavelengths. Figure 7 shows the orientation of the nanoparticles with respect to the incident wave vector (**k**) and electric field ($\mathbf{E}_0$), and the resulting near-field enhancements. For the gold sphere, a strong dipole perpendicular to the wave vector was clearly observed (Figure 7a). For the Au@Ag core−shell polyhedrons, strong dipoles were similarly generated at the two edges, when the incident light was directed along the diagonal of cubic projections of the polyhedrons (Figure 7b−e). Note that there were no significant differences in dipole shapes by changing core geometry, though the near-field enhancement factors varied with the structures. We simulated the polyhedrons with changing the core composition from gold to silver by DDA calculation, but the field enhancements were almost the same as in Figure 7. It indicated that the near-field properties were not very sensitive to the core composition as well as core geometry. It was noteworthy, however, that the far-field properties such as maximum extinction peak positions could be precisely adjusted by altering core morphology, as we discussed previously.

CONCLUSIONS

Heterometallic Au@Ag core−shell nanoparticles were synthesized by a seed-mediated polyol process, which could be extended to a gram scale. The gold core and silver shell morphologies were independently controlled to yield core−shell polyhedral structures. A large blue-shift of the SPR peak was observed in the Au@Ag nanocubes with spherical cores, whereas a strong red-shift peak appeared in the Au@Ag nanocubes with cuboctahedral cores. Such large scale synthesis and morphology and optical property adjustment of heterometallic nanostructures can provide essential units and probes suitable for optoelectronic and biomedical applications.

ASSOCIATED CONTENT

Supporting Information. Experimental details, TEM images, EDX and XRD data, SAED patterns, and DDA simulation results of gold@silver nanopolyhedrons. This material is available free of charge via the Internet at http://pubs.acs.org.

AUTHOR INFORMATION

Corresponding Author

*Tel: +82-42-350-2847. Fax: +82-42-350-2810. E-mail: hsong@kaist.ac.kr, sryu@chosun.ac.kr.

ACKNOWLEDGMENT

This work was supported by the Core Research Program (2010-07592) and the Pioneer Research Program (2008-05103) through the National Research Foundation of Korea funded by the Ministry of Education, Science and Technology. This study was also supported by the research fund from Chosun University 2009.

REFERENCES

(1) Ferrando, R.; Jellinek, J.; Johnston, R. L. *Chem. Rev.* **2008**, *108*, 845–910.
(2) Wang, D.; Li, Y. *Adv. Mater.* **2011**, *23*, 1044–1060.
(3) Kickellbick, G.; Liz-Marzán, L. M. *Encycl. Nanosci. Nanotechnol.* **2004**, *2*, 199–220.
(4) Mulvaney, P.; Giersig, M.; Henglein, A. J. *J. Phys. Chem.* **1993**, *97*, 7061–7064.
(5) Lim, B.; Jiang, M.; Camargo, P. H. C.; Cho, E. C.; Tao, J.; Lu, X.; Zhu, Y.; Xia, Y. *Science* **2009**, *324*, 1302–1305.
(6) Peng, Z.; Yang, H. *J. Am. Chem. Soc.* **2009**, *131*, 7542–7543.
(7) Pazos-Perez, N.; Rodriguez-Gonzalez, B.; Hilgendorff, M.; Giersig, M.; Liz-Marzan, L. M. *J. Mater. Chem.* **2010**, *20*, 61–64.
(8) Lee, W.-r.; Kim, M. G.; Choi, J.-r.; Park, J.-I.; Ko, S. J.; Oh, S. J.; Cheon, J. *J. Am. Chem. Soc.* **2005**, *127*, 16090–16097.
(9) Habas, S. E.; Lee, H.; Radmilovic, V.; Somorjai, G. A.; Yang, P. *Nat. Mater.* **2007**, *6*, 692–697.
(10) Lee, H.; Habas, S. E.; Somorjai, G. A.; Yang, P. *J. Am. Chem. Soc.* **2008**, *130*, 5406–5407.
(11) Fan, F.-R.; Liu, D.-Y.; Wu, Y.-F.; Duan, S.; Xie, Z.-X.; Jiang, Z.-Y.; Tian, Z.-Q. *J. Am. Chem. Soc.* **2008**, *130*, 6949–6951.
(12) Liz-Marzán, L. M. *Langmuir* **2006**, *22*, 32–41.
(13) Liu, M.; Guyot-Sionnest, P. *J. Phys. Chem. B* **2004**, *108*, 5882–5888.
(14) Link, S.; Wang, Z. L.; El-Sayed, M. A. *J. Phys. Chem. B* **1999**, *103*, 3529–3533.
(15) Ma, Y.; Li, W.; Cho, E. C.; Li, Z.; Yu, T.; Zeng, J.; Xie, Z.; Xia, Y. *ACS Nano* **2010**, *4*, 6725–6734.
(16) Cho, E. C.; Camargo, P. H. C.; Xia, Y. *Adv. Mater.* **2010**, *22*, 744–748.
(17) Sánchez-Iglesias, A.; Carbó-Argibay, E.; Glaria, A.; Rodriguez-González, B.; Pérez-Juste, J.; Pastoriza-Santos, I.; Liz-Marzán, L. M. *Chem.—Eur. J.* **2010**, *16*, 5558–5563.
(18) Yoo, H.; Millstone, J. E.; Li, S.; Jang, J.; Wei, W.; Wu, J.; Schatz, G. C.; Mirkin, C. A. *Nano Lett.* **2009**, *9*, 3038–3041.
(19) Xue, C.; Millstone, J. E.; Li, S.; Mirkin, C. A. *Angew. Chem., Int. Ed.* **2007**, *46*, 8436–8439.
(20) Tsuji, M.; Maeda, Y.; Hikino, S.; Kumagae, H.; Matsunaga, M.; Tang, X.; Matsuo, R.; Ogino, M.; Jiang, P. *Cryst. Growth Des.* **2009**, *9*, 4700–4705.
(21) Wu, Y.; Jiang, P.; Jiang, M.; Wang, T.-W.; Guo, C.-F.; Xie, S.-S.; Wang, Z.-L. *Nanotechnology* **2009**, *20*, 305602.
(22) Tsuji, M.; Miyamae, N.; Lim, S.; Kimura, K.; Zhang, X.; Hikino, S.; Nishio, M. *Cryst. Growth Des.* **2006**, *6*, 1801–1807.
(23) Seo, D.; Yoo, C. I.; Jung, J.; Song, H. *J. Am. Chem. Soc.* **2008**, *130*, 2940–2941.
(24) Jung, J.; Seo, D.; Park, G.; Ryu, S.; Song, H. *J. Phys. Chem. C* **2010**, *114*, 12529–12534.
(25) Bohren, C. F.; Huffman, D. R. *Absorption and Scattering of Light by Small Particles*; Wiley: New York, 1983.
(26) Draine, B. T.; Flatau, P. *J. Opt. Soc. Am. A* **1994**, *11*, 1491–1499.
(27) Johnson, P. B.; Christy, R. W. *Phys. Rev. B* **1972**, *6*, 4370–4379.
(28) Seo, D.; Park, J. C.; Song, H. *J. Am. Chem. Soc.* **2006**, *128*, 14863–14870.
(29) Sun, Y.; Xia, Y. *Science* **2002**, *298*, 2176–2179.
(30) Park, J.; An, K.; Hwang, Y.; Park, J.-G.; Noh, H.-J.; Kim, J.-Y.; Park, J.-H.; Hwang, N.-M.; Hyeon, T. *Nat. Mat.* **2004**, *3*, 891–895.
(31) Im, S. H.; Lee, Y. T.; Wiley, B.; Xia, Y. *Angew. Chem., Int. Ed.* **2005**, *44*, 2154–2157.
(32) Wiley, B.; Sun, Y.; Mayers, B.; Xia, Y. *Chem.—Eur. J.* **2005**, *11*, 454–463.
(33) Lu, L.; Wang, H.; Zhou, Y.; Xi, S.; Zhang, H.; Hu, J.; Zhao, B. *Chem. Commun.* **2002**, 144–145.
(34) Gonzalez, C. M.; Liu, Y.; Scaiano, J. C. *J. Phys. Chem. C* **2009**, *113*, 11861–11867.
(35) Mock, J. J.; Barbic, M.; Smith, D. R.; Schultz, D. A.; Schultz, S. *J. Chem. Phys.* **2002**, *116*, 6755–6759.
(36) Kelly, K. L.; Coronado, E.; Zhao, L. L.; Schatz, G. C. *J. Phys. Chem. B* **2003**, *107*, 668–677.